International Journal of Microwave and Wireless Technologies

cambridge.org/mrf

Broadband dual-polarized antenna with parasitic elements for base-station applications

Hamid Zakerifar, Javad Nourinia and Changiz Ghobadi

Department of Electrical Engineering, Urmia University, Urmia, Iran

Research Paper

Cite this article: Zakerifar H, Nourinia J, Ghobadi C (2025). Broadband dual-polarized antenna with parasitic elements for base-station applications. *International Journal of Microwave and Wireless Technologies* 1–11. https://doi.org/10.1017/S175907872400103X

Received: 17 September 2023
Revised: 27 September 2024
Accepted: 3 October 2024

Keywords:
dual-polarized; parasitic element; BTS

Corresponding author: Javad Nourinia;
Email: j.nourinia@urmia.ac.ir

Abstract

A broadband $\pm 45^{\circ}$ dual-polarized base-station antenna based on crossed-dipoles with parasitic elements has been presented in this study. This antenna consists of printed dipoles fed by integrated baluns, parasitic elements, and a ground plane below them. As a result of using parasitic elements on the dipoles and creating a suitable coupling between them, the antenna's impedance bandwidth has been improved, and its dimensions have been reduced. The experimental results show that the proposed antenna can cover the frequency band of 1.58–2.73 GHz with $|S_{11}| < -15$ dB and isolation better than 17 dB. The measured peak gain for the proposed antenna in the frequency band is reported as 7.8 dB. Also, the antenna's half-power beamwidth equals $62.15^{\circ} \pm 1.45^{\circ}$. The proposed antenna is fabricated with overall dimensions of $0.67\lambda_0 \times 0.67\lambda_0 \times 0.17\lambda_0$ and has been measured in the antenna laboratory.

Introduction

As cellular communication has developed in recent years, several communication standards, such as 2G, 3G, and 4G, should be included and designed into a base station to minimize the installation space and reduce cost. A printed antenna with optimal performance and wide beamwidth that can support multiple frequency bands and standards, including Digital Communication System (DCS)/Personal Communication System (PCS)/Universal Mobile Telecommunications System (UMTS)/Long-Term Evolution (LTE), at the same time is in demand and considered a suitable choice for system designers. Printed dipole antennas with integrated balun (balanced-to-unbalanced) feeding can create a wide impedance bandwidth (IBW) with excellent radiation characteristics while having small dimensions and low weight [1]. In recent years, printed dipole antennas with balun feeding have found many applications in Global System for Mobile communication (GSM) systems [2], broadcasting systems [3], Industrial, Scientific, and Medical (ISM) systems [4], and Wireless Local Area Network (WLAN) communications [5]. There are several advantages to using a dipole with balun feeding as a base transceiver station antenna. With balun feeding, dipole antennas provide excellent broadband performance. Their versatility and suitability for applications involving multiple bands make them appropriate for use over various frequencies. The balun transformer ensures that the dipole antenna is fed balanced. As a result of this balanced configuration, common-mode currents, and radiation are reduced, thereby improving antenna efficiency and reducing electromagnetic interference. Furthermore, a dipole antenna exhibits a symmetrical radiation pattern in the horizontal plane, making it ideal for applications requiring uniform coverage. In addition to providing consistent radio coverage over a specific area, this characteristic is advantageous for Base Transceiver Station (BTS) antennas. On the other hand, by supplying a balanced signal to the antenna, the balun minimizes interference and common mode noise, which is essential for BTS antennas since it maintains a high signal-to-noise ratio and ensures reliable communication in the event of external interference. From a practical perspective, this type of antenna can easily be mounted on various structures, including poles, towers, or rooftops. Consequently, it suits different deployment scenarios, allowing optimal coverage and signal propagation. In recent years, the use of balun-fed printed dipole antennas has flourished in BTS systems' configuration. In reference [6], a broadband dual-polarized BTS antenna is introduced, which consists of a crossed-dipole, balun, and ground plane. This design achieves the 1.68–2.74 GHz frequency band with $|S_{11}|$ or $|S_{22}| < -15$ dB criterion and isolation higher than 22 dB. The peak gain of this antenna is 2.8 dB with an overall dimension of $0.84\lambda_0 \times 0.84\lambda_0 \times 0.18\lambda_0$. In reference [7], a filtering antenna Dual-Polarized Filtering Antenna (DPFA) for BTS applications is proposed, capable of overcoming high-order harmonics. This antenna has an IBW of 0.690–1.070 GHz and an isolation of over 35 dB. Furthermore, the antenna has an overall dimension of $0.82\lambda_0 \times 0.82\lambda_0 \times 0.19\lambda_0$ and is reported to have a peak gain of 8.7 dB. Crossed-dipole antennas with coaxial feeds are used in the designs presented in references [8–10]. The BTS antenna, introduced in reference [8], consists of two crossed bow-tie dipoles capable of covering a frequency range of 1.7–2.7 GHz

with isolation of over 30 dB. This antenna has a peak gain of almost 10 dB and occupies a space of $1.47\lambda_0 \times 1.47\lambda_0 \times 0.26\lambda_0$. Antenna performance is improved by parasitic elements in the designs presented in references [9] and [10]. It is possible to have a constructive effect in these designs by taking advantage of the coupling created between the dipole arms and the parasitic elements. The parasitic elements in reference [9] consist of a circular patch cooperating with dipole arms to enhance the radiation properties at high frequencies. On the other hand, the parasitic elements employed in reference [10] shift the first resonance mode to a lower frequency without increasing the antenna size. Other designs have been presented for BTS antennas that use different structures, such as the one introduced in reference [11]. It is a broadband differential patch antenna suitable for a 5G base station. Quasi-trapezoidal patches are the radiating elements, capacitively driven by two trapezoidal feeding structures. It is worth mentioning that the design and optimization of parasitic elements near the dipole arms with magnetic coupling can be challenging. It is necessary to carefully consider coupling effects, element size, spacing, and electrical properties to achieve bandwidth enhancement, size reduction, and other improvements.

In recent years, several dual-polarized dual-band antennas with new techniques have been introduced [12–21]. These antennas can be classified into three groups according to the separation of their frequency bands. The first category operates at sub-6G and millimeter-wave frequencies through metasurfaces and specific antenna arrangement schemes. The second category of these antennas operates at two widely separated frequency bands within the standard BTS systems frequency ranges, specifically 0.69–0.96 GHz, 1.7–2.7 GHz, and 3.3–5 GHz. The third group comprises antennas operating in adjacent frequency bands, introducing a more complex design challenge.

This study utilized arrow-shaped parasitic elements to enhance the IBW and reduce the antenna's overall dimension. The proposed broadband $\pm 45^\circ$ dual-polarized base-station antenna comprises printed slotted diamond-shaped crossed-dipole, parasitic elements, and a square ground plane. Integrated baluns feed the dipoles, and two coaxial cables transmit the signal to the baluns. According to the measurements, the proposed antenna has a wide IBW of 53.26% with $|S_{11}|$ or $|S_{22}| < -15$ dB and a 3-dB beamwidth of $62.15^\circ \pm 1.45^\circ$.

Antenna configuration

In the design presented in this work, the configuration of printed dipole antennas with integrated balun feeding is used. These antennas have wide bandwidth and stable and acceptable radiation behavior [22–25]. The antenna configuration proposed in this study is demonstrated in Fig. 1.

Slotted diamond-shaped dipole arms and arrow-shaped parasitic elements are used in this design. This figure shows an FR4 substrate with a relative permittivity of 4.4, a loss tangent of 0.02, and a thickness of 1 mm with dipole arms and parasitic elements printed on the bottom and top layers, respectively. This substrate is located at the top of the antenna. It is possible to achieve the cross-shaped arrangement of the baluns related to the dipoles by creating slots above and below the two FR4 substrates with a thickness of 0.8 mm in the middle part of the antenna. Baluns are soldered to the dipole arms from the top and the ground plane from the bottom. Also, an FR4 substrate with a thickness of 0.8 mm is located in the lower portion of the antenna, which supports other parts mechanically and establishes the ground plane on both sides. The input signals are transmitted to the antenna through two coaxial cables soldered from the bottom of the lower substrate to the antenna. Thus, the external conductors of the coaxial cables are soldered to the ground plane of the substrate, and the internal conductors are soldered to the Γ-shaped feeding of the baluns after passing through two holes in the substrate. The baluns proposed in this paper consist of a Γ-shaped feed on one side of the substrate, and also, there are two shorted patches that serve as a slot line on the other side of the substrate. The input signal to the Γ-feed is coupled from the horizontal part to the slot line, where it reaches the dipole arms. Consequently, dipoles-1 and -2 are placed orthogonally on each other, and because dipoles are linearly polarized, they produce horizontal and vertical linear polarization. On the other hand, by rotating the antennas by 45°, the $\pm 45^\circ$ slant polarizations are formed.

Designing a printed dipole antenna with integrated balun for BTS applications in the 1.7–2.7 GHz frequency range involves several equations and calculations. The dimensions of the antenna segments are critical to ensure proper operation within the specified frequency range. In the first step, the center frequency of the design should be determined. The proposed antenna in this work should cover the frequency range 1.7–2.7 GHz for BTS applications. The central frequency (f_0) can be taken as the average of this range:

$$f_0 = \frac{f_l + f_h}{2} = \frac{1.7 + 2.7}{2} = 2.2\,GHz \tag{1}$$

So, the wavelength (λ) corresponding to the central frequency (f_0) is equal:

$$\lambda = \frac{c}{f_0} = \frac{3 \times 10^8}{2.2 \times 10^9} \approx 136\,mm \tag{2}$$

where c is the speed of light. Consequently, for a half-wave dipole, each arm length is approximately:

$$L = \frac{\lambda}{4} = \frac{136}{4} = 34\,mm \tag{3}$$

However, due to the effects of the dielectric substrate and the actual operational environment, the effective length might be slightly shorter. Typically, corrections are made for the substrate's effective dielectric constant (ε_r). In the presented design, the diamond-shaped dipole arms are connected from the middle to the short-circuited patches of the balloon, so their length is proportional to the provided equations. However, parametric studies have also been conducted to obtain the optimal parameters.

In the second step, the dimension of the balun should be calculated. The balun is designed to convert the unbalanced coaxial feed line to a balanced antenna. The balun can be integrated with the dipole on the same substrate. Commonly used substrates for printed antennas include FR4, Rogers, and other materials with known dielectric constants (ε_r). The choice of substrate affects the dimensions due to the effective wavelength in the substrate. For microstrip lines, the effective dielectric constant influences the effective wavelength (λ_{eff}). Assuming a dielectric substrate with $\varepsilon_r = 4.4$ (for example FR4):

$$\lambda_{eff} = \frac{\lambda}{\sqrt{\varepsilon_{eff}}} \tag{4}$$

where:

$$\varepsilon_{eff} = \frac{\varepsilon_r + 1}{2} = \frac{4.4 + 1}{2} = 2.7 \tag{5}$$

Therefore:

$$\lambda_{eff} = \frac{136}{\sqrt{2.7}} = 83\,mm \tag{6}$$

https://doi.org/10.1017/S175907872400103X Published online by Cambridge University Press

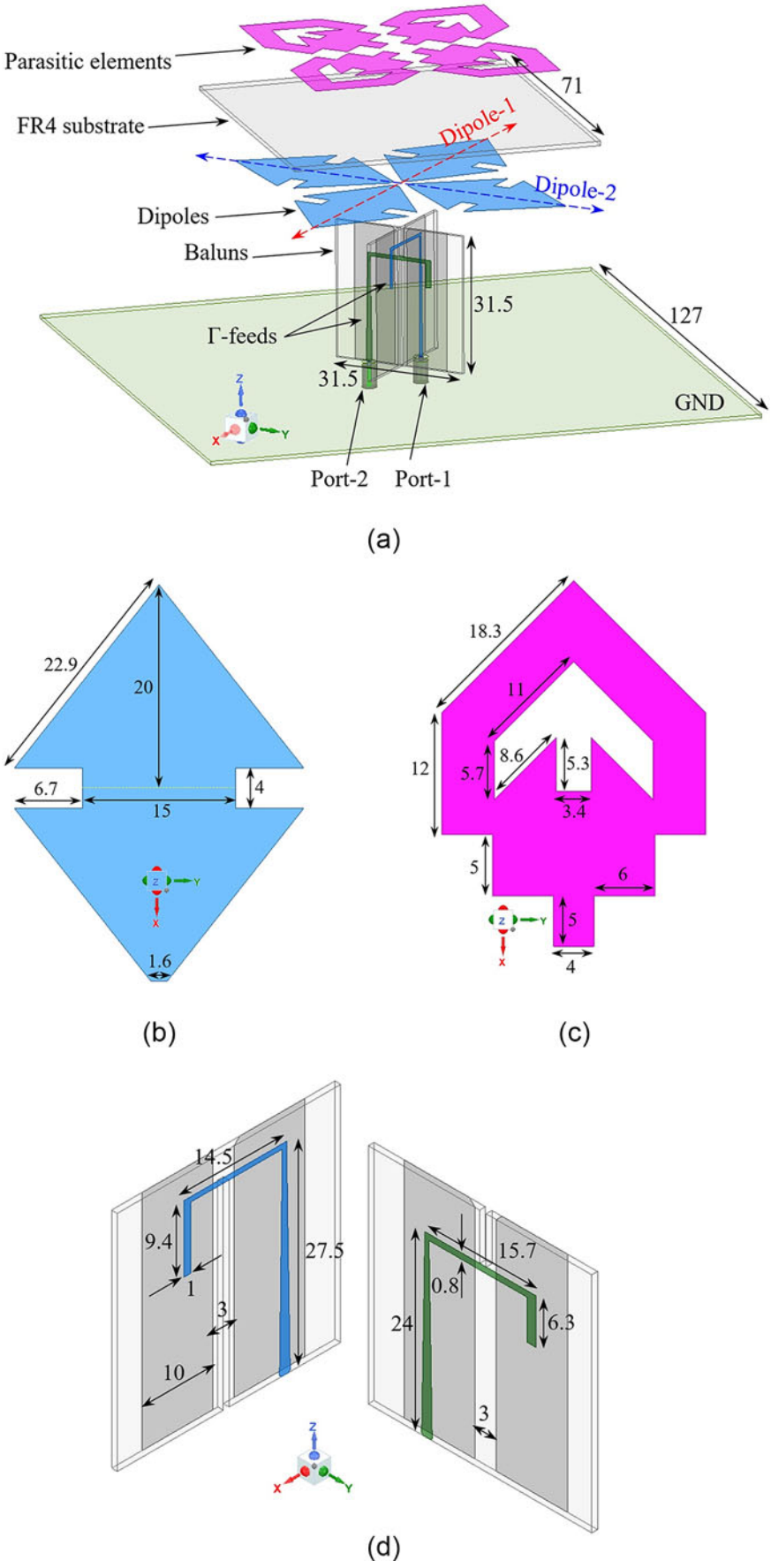

Figure 1. (a) 3D view of the proposed antenna, (b) dipole arms, (c) parasitic elements, and (d) balun structures. (All dimensions are in millimeters).

https://doi.org/10.1017/S175907872400103X Published online by Cambridge University Press

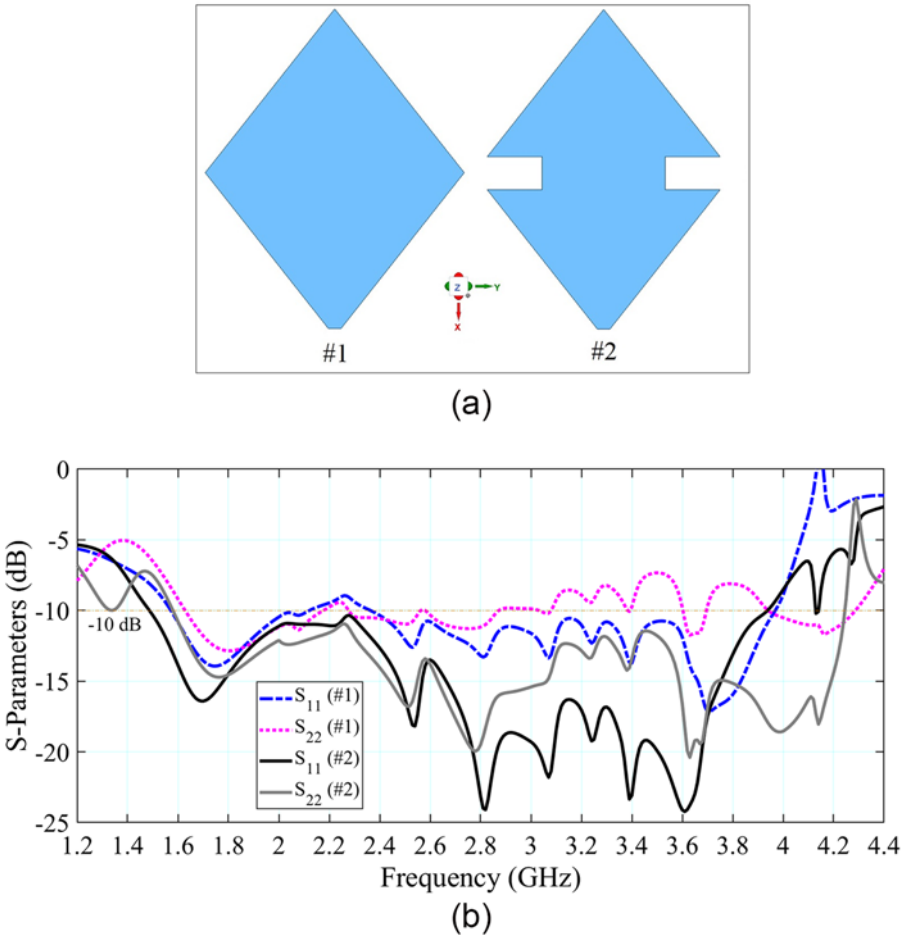

Figure 2. (a) Two configurations for dipole arms (#1 and #2) and (b) S-parameters of the antenna for configurations of #1 and #2 for dipole arms.

Consequently, the effective length of the dipole arms should be equal to:

$$L_{eff} = \frac{\lambda_{eff}}{4} = \frac{83}{4} = 21\,mm \tag{7}$$

These calculations provide a starting point. The optimal dimensions should be reconsidered through simulation and parametric studies to account for additional factors, such as nearby structures (parasitic elements in this work), precise substrate characteristics, and feed structure (including balun and connector).

Antenna without parasitic elements

At first, the aim was to design a crossed-dipole antenna capable of producing dual polarization. The dipole arms were initially configured in a diamond-shaped formation, as shown in Fig. 2(a). As a result of the parametric analysis, it has been decided to modify this shape into a slotted diamond-shape. According to the investigation, the modifications made to the dipole arms have enabled a suitable bandwidth for the antenna. This results in a frequency bandwidth of 1.48–3.93 GHz and 1.57–4.24 GHz, respectively, for the crossed-dipole antennas in ports -1 and -2. Figure 2(b) illustrates the results of the simulations performed on the antenna with both structures introduced for the dipole arms.

Additionally, it is crucial to investigate the configuration of the Γ-feed. A detailed analysis of this issue can be found in Fig. 3.

Based on this figure, two modes of the Γ-feeding can be considered, the uniform mode and the modified mode (proposed). Simulated results demonstrate the superiority of the modified mode over the uniform mode, and the IBW is obtained as before. The bandwidth has a criterion of $|S_{11}|$ or $|S_{22}| < -10$ dB, which does not meet the requirements of BTS systems. As a result, a further step needs to be taken in antenna design to increase the IBW sufficiently. According to Figs. 1(d) and 3, the dimensions of two Γ-feeds have been chosen differently in order to prevent a connection between them and the possibility of them passing over one another, but the difference in sizes has been taken into account in such a way that impedance matching and operational bandwidth to the results obtained in each antenna port are similar.

Theoretical foundations and physics of antenna design

An antenna's IBW is defined as the frequency range over which the reflection coefficient $|S_{11}|$ is less than a certain threshold, commonly −10 dB. However, the threshold is more stringent at −15 dB in this case. Generally, the reflection coefficient $|S_{11}|$ is related to the input impedance Z_{in} of the antenna as follows:

$$|S_{11}| = \left|\frac{Z_{in} - Z_0}{Z_{in} + Z_0}\right| \tag{8}$$

In this case, Z_0 represents the characteristic impedance of the feed line, which is usually 50 Ω. Z_{in} must remain close to Z_0 over a wide frequency range, minimizing $|S_{11}|$ and thus enhancing IBW. The parasitic elements are passive structures not directly fed from

https://doi.org/10.1017/S175907872400103X Published online by Cambridge University Press

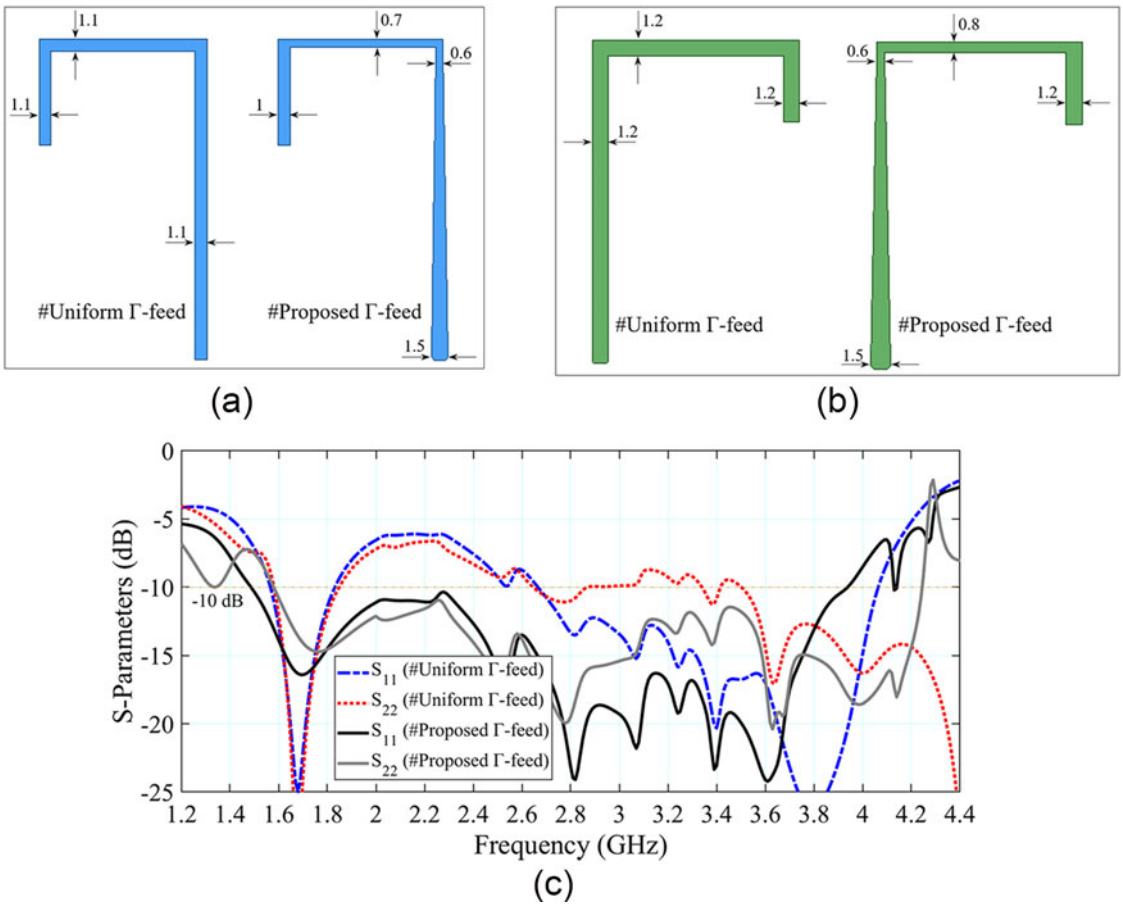

Figure 3. Two configurations for Γ-feed (#uniform Γ-feed and #proposed Γ-feed), in (a) dipole-1, (b) dipole-2, and (c) S-parameters of the antenna for two configurations for Γ-feed. (All dimensions are in millimeters).

the antenna's feed line but are in contact with the driven elements (the dipoles) via mutual coupling. Their effects can significantly impact the antenna's input impedance and radiation characteristics. The resonant frequency f_r of a dipole antenna is determined by its length L and the effective wavelength λ_{eff}:

$$f_r \approx \frac{c}{2L\sqrt{\varepsilon_{eff}}} \tag{9}$$

where c is the speed of light in free space, and ε_{eff} is the effective dielectric constant of the substrate. The presence of parasitic elements near dipoles leads to additional resonances due to their own geometry and coupling with the dipoles. Depending on their placement and dimensions, these parasitic elements can either enhance or suppress specific resonant modes. The mutual coupling between a driven dipole and a parasitic element can be analyzed using the mutual impedance Z_{12}:

$$Z_{12} = \int_{V_1}\int_{V_2} J_1 \cdot E_2 \, dV_1 \, dV_2 \tag{10}$$

where J_1 is the current density on the driven element, and E_2 is the electric field produced by the parasitic element. The formula provided for mutual impedance is a general expression used to describe the interaction between two antennas (or antenna elements), such as a driven dipole and a parasitic element (in this case). In the context of this formula, V_1 denotes the volume over which the current density J_1 is distributed on the driven element (the dipole arms in this case). The volume V_1 covers the region occupied by the driven dipole, including any significant portions of the near-field where the electromagnetic fields generated by the dipole are strong. Similarly, V_2 represents the volume over which the parasitic element's electric field E_2 is considered. This volume encompasses the region occupied by the parasitic element, including the areas characterized by electromagnetic fields. Furthermore, J_1 represents the current density on the driven element (dipole). It is a vector quantity describing the distribution and magnitude of the current flowing on the surface of the driven element, and E_2 refers to the electric field generated by the parasitic element. This field is a result of the currents induced in the parasitic element by the electromagnetic fields originating from the driven element (dipole). Furthermore, dV_1 and dV_2 represent differential volume elements within the volumes V_1 and V_2. The integrals sum up the contributions of the mutual coupling over the entire volumes where the fields and currents are present.

On the other hand, the mutual impedance Z_{12} quantifies the interaction between the two elements (driven and parasitic elements) by integrating the product of the current density on the driven element and the electric field generated by the parasitic element over the volumes V_1 and V_2. As a result of this interaction, the overall impedance of the driven dipole is affected, which in turn affects the performance of the antenna, such as its IBW and radiation pattern. It is essential to understand and calculate the mutual impedance Z_{12} in this design. It enables the determination of how

https://doi.org/10.1017/S175907872400103X Published online by Cambridge University Press

parasitic elements affect the input impedance of the driven dipole, and by extension, the antenna's operating characteristics. The total input impedance Z_{in} of the antenna becomes:

$$Z_{in} = Z_d + Z_{12} \tag{11}$$

where Z_d is the self-impedance of the driven dipole. The parasitic elements, when optimally designed and positioned, can make additional resonant paths and increase the total adequate bandwidth of the antenna. This is because they allow the antenna system to support multiple resonant modes at slightly different frequencies, which combine to achieve a broader overall resonance. Based on the derivative of the impedance concerning frequency, it is possible to estimate the total IBW:

$$IBW \propto \left(\frac{d\,|Z_{in}|}{df}\right)^{-1} \tag{12}$$

Z_{in} is smoothed out over a wider frequency range by the introduction of parasitic elements, thereby reducing the sharp variations that would otherwise limit its bandwidth. Parasitic elements can also be used to reduce the physical size of an antenna without compromising its performance. As a result of carefully choosing the shape and location of parasitic elements (in this case, arrow-shaped), the effective electrical length of the dipoles can be increased, allowing the antenna to resonate at a lower frequency than a simple dipole of the same physical dimensions. This is mathematically represented by an effective length L_{eff} of the dipole, which is extended by the parasitic elements:

$$L_{eff} = L + \Delta L_p \tag{13}$$

where ΔL_p is the contribution from the parasitic elements. Consequently, the antenna can maintain its resonant frequency at a given size or achieve the same frequency with a reduced size:

$$f_r \propto \frac{1}{L_{eff}} \tag{14}$$

Parasitic elements also affect the radiation pattern and gain. The parasitic elements can create constructive and destructive interference patterns, which can affect the total radiated power Prad and the directivity D of the antenna. An antenna's gain G can be calculated as follows:

$$G = D \times \eta \tag{15}$$

where η represents the antenna's efficiency. Parasitic elements can modify the current distribution on dipoles, increasing directivity and thus increasing gain in certain directions. Simulations (e.g., using High-Frequency Structure Simulator (HFSS) or Computer Simulation Technology (CST)) and experimental measurements are often used to validate the effects of parasitic elements on impedance and bandwidth. Typically, the design process involves iterating the geometry and placement of parasitic elements in order to achieve the desired IBW, gain, and overall performance. By introducing additional resonant modes and smoothing the impedance variation over frequency, parasitic elements increase the IBW. As a result, the antenna's physical dimensions can be reduced by increasing the electrical length of the dipoles. Parasitic elements can enhance the gain and shape the radiation pattern by altering the current distribution and mutual coupling effects.

Proposed antenna, results, and discussion

Examining the concept of magnetic coupling between the dipole arms and the parasitic elements is necessary to understand how the parasitic elements work. In this section, the performance of the proposed antenna is investigated by employing parasitic elements. Magnetic coupling in a dipole antenna can improve its bandwidth and reduce its dimensions. This technique is known as "mutual coupling" or "inductive coupling." The magnetic field generated by the current flowing through the dipole induces currents in parasitic elements when placed near the dipole arms. If certain conditions arise, the induced currents will interact with the currents in the dipole arms constructively, resulting in a broader frequency response, expanding the IBW of the antenna and allowing it to operate over a more comprehensive range of frequencies. Consequently, the antenna's effective length can be increased by employing parasitic elements without physically extending the dipole arms. Therefore, it allows for a more compact antenna design while maintaining resonant characteristics. It is concluded that the interaction between the parasitic elements and dipole arms effectively extends the antenna's electrical length, reducing the dipole's physical dimensions and making the antenna more compact. Figure 4 compares the antenna's IBW with and without parasitic elements.

Concerning the figure, it is clear that the presence of parasitic elements next to the dipole arms significantly increases the IBW of the antenna with the criterion of $|S_{11}|$ or $|S_{22}| < -15$ dB. Meanwhile, parasitic elements are necessary for the proposed antenna to satisfy this criterion regarding IBW. Based on the simulation results, it can be found that utilizing parasitic elements in the proposed antenna structure makes the antenna can cover the frequency ranges of 1.53–3.03 GHz and 1.55–2.93 GHz for ports -1 and -2, respectively, with a criterion of $|S_{11}|$ or $|S_{22}| < -15$ dB. It is also essential in antenna theory to study the distribution of surface currents on dipole arms and parasitic elements. This analysis is necessary to understand an antenna system's behavior and performance. The surface current distribution on the proposed antenna with and without parasitic elements is depicted in Fig. 5. It can be seen in

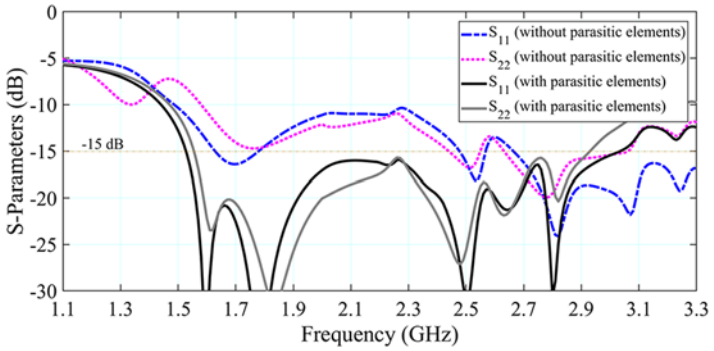

Figure 4. S-parameters of the proposed antenna with/without parasitic elements.

https://doi.org/10.1017/S175907872400103X Published online by Cambridge University Press

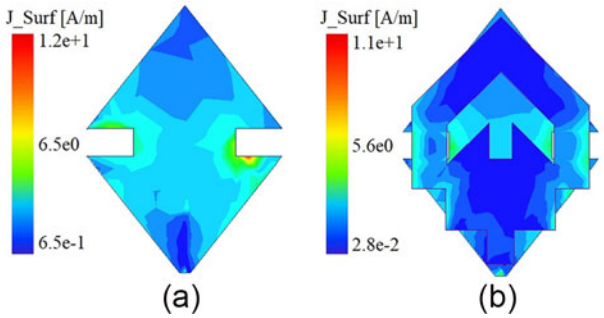

Figure 5. Current distribution on the (a) proposed antenna without parasitic elements and (b) with parasitic elements.

the figure that the accumulation of surface currents on the dipoles in which parasitic elements are not present is more accumulated in the slot sections. In addition, when parasitic elements are added to an antenna structure, some of the surface currents are also generated on the parasitic elements, increasing antenna IBW. To better understand this phenomenon, we also analyzed the impedance of the proposed antenna.

The input impedance of an antenna is a complex quantity with real and imaginary parts that characterize the opposition to the current flow in an electrical circuit model. In the case of a dipole antenna, the impedance consists of a resistive component (real part) and a reactive component (imaginary part). Indeed, the power loss is represented by the resistive component of the impedance and is denoted by the real part of the impedance, typically measured in ohms. Several factors contribute to the real part, including the resistance of the conductive elements, losses in the antenna structure, and radiation resistance. Instead, the impedance's reactive component represents the energy storage and release in the antenna. Similarly, it is measured in ohms and represents the imaginary part of the impedance. Depending on the frequency of operation and the physical characteristics of the antenna, the reactance can either be capacitive or inductive. As a result, a dipole antenna's overall impedance is determined by the cooperation of resistance and reactance, which is essential to have a thorough understanding of both components to optimize the dipole antenna's performance. Considering the physical dimensions, spacing, and electrical properties of the parasitic element, its effect on the impedance of the dipole can be taken into account. In addition, analytical methods using electromagnetic field analysis techniques can provide valuable insights into the impedance behavior of the parasitic element. Parasitic elements can be analyzed using electromagnetic simulation software such as the HFSS package. Using numerical methods, the software tools solve Maxwell's equations and simulate the behavior of electromagnetic fields in the antenna system. The impedance values of the proposed antenna with and without parasitic elements are plotted in Fig. 6 regarding real and imaginary parts.

The simulation results show that the real and imaginary parts of the antenna input impedance in the presence of parasitic elements are more inclined to the values of 50Ω and 0Ω, respectively, and show better impedance matching.

Antenna fabrication and measurement results

Antennas in base stations may require a wide bandwidth in modern mobile communication systems. For example, 2G/3G/4G/LTE systems operating in the 2 GHz band must cover the frequency

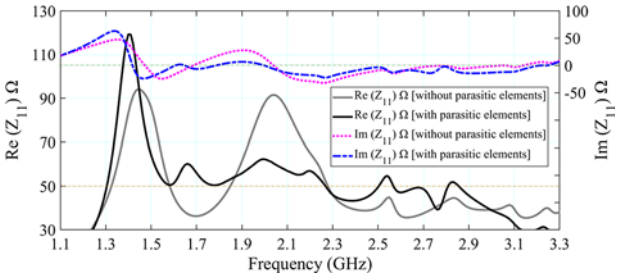

Figure 6. The impedance (real and imaginary parts) of the proposed antenna with/without parasitic elements.

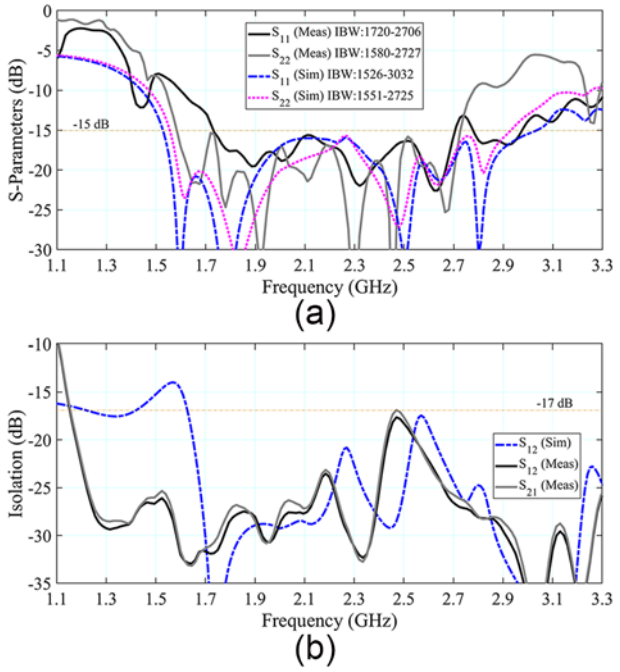

Figure 7. Simulated and measured S-parameters of the proposed antenna, (a) impedance bandwidth, and (b) isolation.

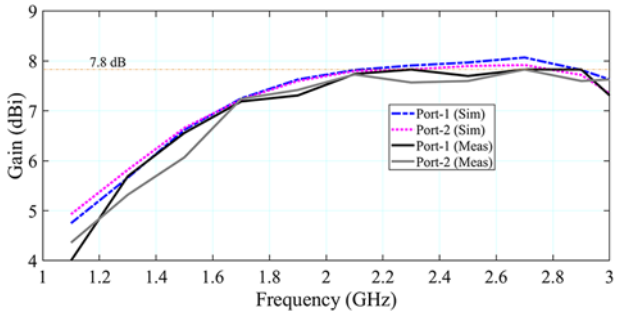

Figure 8. Simulated and measured realized gain of the antenna.

range of 1.71–2.69 GHz, that is, 2G (1710–1920 MHz), 3G (1880–2170 MHz), and 4G/LTE (2300–2400 MHz and 2570–2690 MHz). As illustrated in Fig. 7(a), a comparison between the measured and simulated IBWs of the proposed BTS antenna is presented. Experimental results show this design can cover 1.72–2.71 GHz and 1.58–2.72 GHz frequency bands with $|S_{11}|$ or $|S_{22}| < -15$ dB criterion for ports-1 and -2, respectively.

https://doi.org/10.1017/S175907872400103X Published online by Cambridge University Press

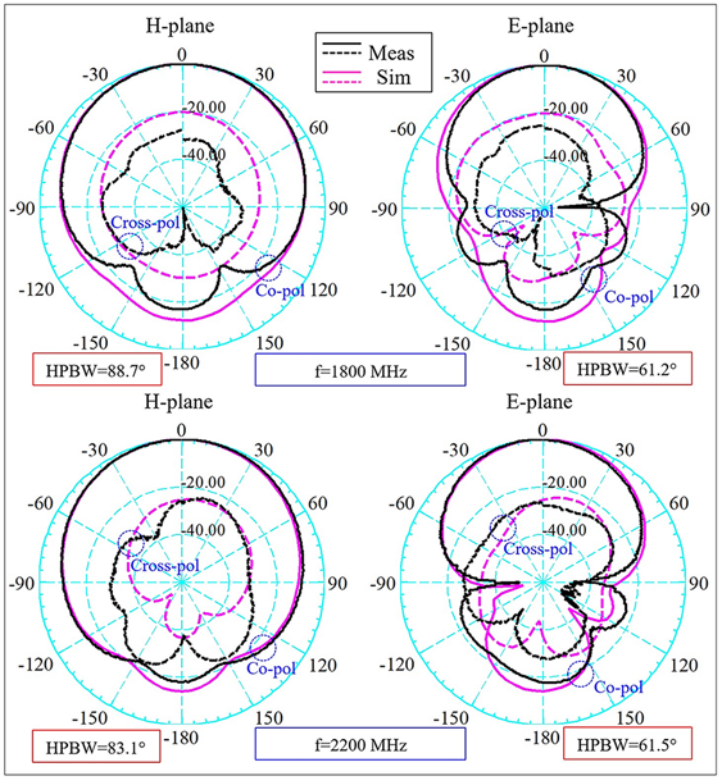

Figure 9. Simulated and measured normalized H- and E-plane radiation patterns of the proposed antenna for (a) port-1 and (b) port-2.

Furthermore, as reported in Fig. 7(b), the simulated and measured isolations ($-|S_{12}|$ and $-|S_{21}|$ in dB) are higher than 17 dB in the operating frequency band. The proposed antenna employs a crossed-dipole configuration, which inherently has dual polarization. This design allows the antenna to exhibit $\pm 45^{\circ}$ slant polarizations (or vertical/horizontal linear polarizations as an

https://doi.org/10.1017/S175907872400103X Published online by Cambridge University Press

alternative) by positioning the two orthogonally placed dipoles at $\pm 45^{\circ}$ to the horizontal plane (or 0° and 90°).

These slant polarizations are crucial in BTS applications as they minimize polarization mismatch and enhance signal reception in environments with multipath propagation. Furthermore, when aligned with the vertical and horizontal axes, the antenna can also function with V/H linear polarizations, providing versatility in various operational scenarios. We have confirmed the dual-polarization performance through experimental measurements, demonstrating excellent isolation between the two polarizations. In addition, the proposed antenna has a measured peak gain of 7.8 dB in the operating frequency band. Figure 8 shows the simulated and measured results of the proposed BTS antenna gain in ports-1 and -2.

In this work, all the simulated results were extracted using HFSS Version 15 software, and the experiments were carried out using an Agilent E8363C network analyzer. The numerical and experimental results show a good agreement, and, in some frequencies, there is a slight discrepancy between the numerical and experimental results due to errors made during antenna fabrication and testing. Simulated and measured normalized H- and E-plane radiation patterns of the proposed antenna for ports-1 and -2 are plotted in Fig. 9.

The patterns are extracted at two frequencies of 1800 and 2200 MHz based on co- and cross-poles. According to the results, the proposed BTS antenna has measured half-power beamwidths (HPBWs) of $62.15^{\circ} \pm 1.45^{\circ}$ at two sample frequencies. Furthermore, using a smooth ground plane under the antenna makes its radiation pattern unidirectional at both planes. Following the design and optimization of the proposed BTS antenna, it was fabricated using FR4 substrates and tested in the antenna laboratory. Photographs of the antenna prototype made in this work are shown in Fig. 10. This figure also depicts how to test the antenna's S-parameters using a network analyzer and its radiation parameters using an anechoic chamber.

The proposed BTS antenna offers significant advantages and is superior to similar works regarding bandwidth and dimensions. In addition, due to its smaller dimensions, it is more flexible in installation, making it suitable for various environments and reducing the visual impact. With increased bandwidth and compact size, BTS installations are not only able to optimize network performance but also enhance their aesthetic appeal. The results of this comparison are tabulated in Table 1.

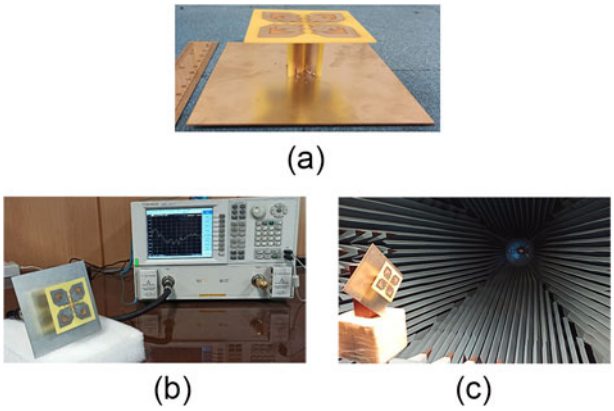

Figure 10. Photographs of the (a) manufactured prototype, (b) antenna connected to the Vector Network Analyzers (VNA), and (c) antenna at an anechoic chamber.

The proposed theory in this work on printed dipole antennas with integrated baluns and Γ-shaped feed elements could be extended in future research. The authors appreciate the reviewers' suggestion to explore our proposed model's future potential and extensions. Several avenues for further research could enhance the impact and relevance of our work on printed dipole antennas with integrated baluns and Γ-shaped feed elements.

Fundamentally, future work could explore adapting our antenna design to support wideband or multiband operation. By optimizing the geometric parameters and incorporating additional elements, the antenna could be made to operate efficiently across multiple frequency bands, such as those used in modern communication systems (e.g., 5G, Wi-Fi, IoT). Furthermore, scaling the design for higher frequency bands, such as millimeter-wave frequencies (24–100 GHz), could be investigated. This technique addresses challenges related to increased losses and manufacturing precision at higher frequencies. Also, integrating active components, such as high frequency diodes, varactors, or MEMS switches, can lead to reconfigurable antennas capable of dynamically adjusting their frequency, polarization, radiation pattern, and gain.

Table 1. Comparison of antenna measured results

Ref.	IBW (GHz)	Isolation (dB)	Peak gain (dB)	HPBW (°)	Size (λ_0^3)	Technique
[6]	(48%) 1.68–2.74 ($S11 < -15$ dB)	>22 dB	8.2	62.5 ± 3.5	0.84 × 0.84 × 0.18	Crossed-dipole with balun feeding
[7]	(43.2%) 0.69–1.07 ($S11 < -15$ dB)	>35 dB	8.7	68.8 ± 2.1	0.82 × 0.82 × 0.19	Crossed-dipole with balun feeding
[8]	(45%) 1.7–2.7 ($S11 < -15$ dB)	>30 dB	∼10	∼65	1.47 × 1.47 × 0.26	Bow-tie dipole fed by a coaxial line
[9]	(100%) 1.7–5.1 ($S11 < -10$ dB)	>20 dB	8.9	65 ± 5	0.79 × 0.79 × 0.21	Crossed-dipole & parasitic element
[10]	(44.54%) 1.71–2.69 (Voltage Standing Wave Ratio (VSWR) < 1.65)	>28 dB	9.2	64.8 ± 2.7	0.83 × 0.83 × 0.20	Crossed-dipole & parasitic element
[11]	(27.8%) 3.19–4.22 (Voltage Standing Wave Ratio (VSWR) < 1.5)	>39.5 dB	9.35	∼65	0.92 × 0.92 × 0.12	Quasi-trapezoidal patches
This work	(53.26%) 1.58–2.73 ($S11 < -15$ dB)	>17 dB	7.8	62.15 ± 1.45	0.67 × 0.67 × 0.17	Crossed-dipole & parasitic element

https://doi.org/10.1017/S175907872400103X Published online by Cambridge University Press

This could provide greater flexibility and adaptability for various applications.

Conclusion

A broadband dual-polarized antenna with parasitic elements for base-station applications is proposed and investigated in this work. The main contribution of this work is that offers an excellent solution that addresses the challenges of IBW enhancement and overall dimension reduction. Through the implementation of parasitic elements in the proposed design, the antenna's overall size can be reduced, as well as producing a wide IBW of 1.58–2.73 GHz with $|S_{11}| < -15$ dB and isolation better than 17 dB.

Acknowledgements. The authors would like to acknowledge the technical assistance provided by Northwest Antenna and Microwave Research Laboratory (NAMRL) at Urmia University.

Competing interests. The authors declare that they have no known competing financial interests or personal relationships that could have appeared to influence the work reported in this paper.

References

1. **Li R, Wu T, Pan B, Lim K, Lasker J and Tentzeris MM**. and (2009) Equivalent-circuit analysis of a broadband printed dipole with adjusted integrated balun and an array for base station applications. *IEEE Transactions on Antennas and Propagation* **57**, 2180–2184.
2. **Hatamian A, Ghobadi C, Nourinia J and Shokri M** (2022) A compact triple-band printed dipole antenna using C-shaped resonators with stable radiation for GSM/ISM/WLAN applications. *Microwave and Optical Technology Letters* **65**, 611–618.
3. **Teimouri MH, Ghobadi C, Nourinia J, Kaboutari K, Shokri M and Virdee BS** (2022) Broadband printed dipole antenna with integrated balun and tuning element for DTV application. *AEU - International Journal of Electronics and Communications* **148**, 154161.
4. **Nasirzade R, Nourinia J, Ghobadi C, Shokri M and Naderali R** (2020) Broadband printed MIMO dipole antenna for 2.4 GHz WLAN applications. *Journal of Instrumentation* **15**, 01.
5. **Shokri M, Faeghi P, Kaboutari K, Ghobadi C, Nourinia J, Amiri Z and Barzegari R** (2021) A printed dipole antenna for WLAN applications with anti-interference functionality. In *2021 Photonics & Electromagnetics Research Symposium (PIERS)*, IEEE, 1486-1494.
6. **Huang H, Liu Y and Gong S** (2017) A broadband dual-polarized base station antenna with sturdy construction. *IEEE Antennas and Wireless Propagation Letters* **16**, 665–668.
7. **Chang Y and Chu Q** (2020) Dual-polarized filtering antenna with harmonic suppression for base station applications. *Microwave and Optical Technology Letters* **62**, 2033–2039.
8. **Cui Y, Li R and Fu H** (2014) A broadband dual-polarized planar antenna for 2G/3G/LTE base stations. *IEEE Transactions on Antennas and Propagation* **62**, 4836–4840.
9. **Ye LH, Ye DG, Chen Z and Li JF** (2023) Ultra-wideband dual-polarized base-station antenna with stable radiation pattern. *IEEE Transactions on Antennas and Propagation* **71**, 1919–1924.
10. **Zheng D, Luo Y and Chu Q-X** (2020) A miniaturized wideband dual-polarized antenna based on mode-control principle for base-station applications. *IEEE Access* **8**, 62218–62227.
11. **Guan X, Zhang X, Ren B and Wang C** (2022) A broadband dual-polarized antenna with quasi-trapezoidal patches for 5G base station application. *International Journal of RF and Microwave Computer-Aided Engineering* **32**(10), e23309. https://doi.org/10.1002/mmce.23309
12. **Li Y and Chu Q-X** (2021) Coplanar dual-band base station antenna array using concept of cavity-backed antennas. *IEEE Transactions on Antennas and Propagation* **69**, 7343–7354.
13. **Zhu Y, Chen Y and Yang S** (2020) Integration of 5G rectangular MIMO antenna array and GSM antenna for dual-band base station applications. *IEEE Access* **8**, 63175–63187.
14. **Zhu Y, Chen Y and Yang S** (2020) Helical torsion coaxial cable for dual-band shared-aperture antenna array decoupling. *IEEE Transactions on Antennas and Propagation* **68**, 6128–6135.
15. **Yang SJ, Yanga Y and Zhang XY** (2021) Low scattering element-based aperture-shared array for multiband base stations. *IEEE Transactions on Antennas and Propagation* **69**, 8315–8324.
16. **Sun -H-H, Zhu H, Ding C, Jones B and Guo YJ** (2020) Scattering suppression in a 4G and 5G base station antenna array using spiral chokes. *IEEE Antennas and Wireless Propagation Letters* **19**, 1818–1822.
17. **He D, Yu Q, Chen Y and Yang S** (2021) Dual-band shared-aperture base station antenna array with electromagnetic transparent antenna elements. *IEEE Transactions on Antennas and Propagation* **69**, 5596–5606.
18. **Liu Y, Wang S, Li N, Wang J-B and Zhao J** (2018) A compact dual band dual-polarized antenna with filtering structures for sub-6 GHz base station applications. *IEEE Antennas and Wireless Propagation Letters* **17**, 1764–1768.
19. **Jia F, Liao S and Xue Q** (2020) A dual-band dual-polarized antenna array arrangement and its application for base station antennas. *IEEE Antennas and Wireless Propagation Letters* **19**, 972–976.
20. **Wen D, Cao YF, Pan YM, Chen ZX and Zhang XY** (2019) Compact dual-band dual-polarized base-station antenna array with a small frequency ratio using filtering elements. *IEEE Access* **7**, 127800–127808.
21. **Li J-F, Wu D-L, Zhang G, Wu Y-J and Mao C-X** (2019) Compact dual polarized antenna for dual-band full-duplex base station applications. *IEEE Access* **7**, 72761–72769.
22. **Shokri M, Ghobadi C and Nourinia J** (2023) Dual-band circularly polarized asymmetric dipole array antenna for GPS L1 and L2 bands. *AEU - International Journal of Electronics and Communications* **169**, 154753.
23. **Barzegari R, Ghobadi C, Nourinia J and Shokri M** (2023) A dual-band dipole array antenna with fan-beam characteristics for C- and X-band applications. *IEEE Access* **11**, 67330–67338.
24. **Shirzad H, Ghobadi C, Nourinia J, Shokri M and Karamirad M** (2024) Single layer multi-band transmissive type linear to circular polarization converter with wide angular stability for C-, X-, and Ku-band applications. *IEEE Access* **12**, 14083–14093.
25. **Gou Y, Yang S, Li J and Nie Z** (2014) A compact dual-polarized printed dipole antenna with high isolation for wideband base station applications. *IEEE Transactions on Antennas and Propagation* **62**, 4392–4395.

Hamid Zakerifar was born in July, 1989 in Iran. He received his M.Sc. degrees in Electrical Engineering from ECE Department, K. N. Toosi University of Technology, Tehran, Iran. He is currently a Ph.D. candidate of Telecommunication Engineering in Urmia University, Urmia, Iran. Her research interests include multiband and broadband antenna and power divider design.

Javad Nourinia received his B.Sc. in Electrical and Electronic Engineering from Shiraz University, M.Sc. degree in Electrical and Telecommunication Engineering from Iran University of Science and Technology, and Ph.D. degree in Electrical and Telecommunication from University of Science and Technology, Tehran, Iran, in 2000. He has been the Head of the Faculty Engineering Department from 2013 to 2017 and a Distinguished Professor at Urmia University. He has been included in the Top One Percent of the World's Scientists and Academics according to Thomson Reuters' list since 2016. His research interests include small antennas, filters, MIMO antennas, periodic structures, optimization, and measurement.

https://doi.org/10.1017/S175907872400103X Published online by Cambridge University Press

Changiz Ghobadi received his B.Sc. in Electrical Engineering and M.Sc. degrees in Electrical Engineering Telecommunication from Isfahan University of Technology, Isfahan, Iran, and Ph.D. degree in Electrical Telecommunication from University of Bath, Bath, UK, in 1998. He is currently a Professor in the Department of Electrical Engineering of Urmia University, Urmia, Iran. He has supervised and administered more than 130 M.Sc. and 32 Ph.D. students and their thesis. He has authored and coauthored over 360 scientific publications including accredited journals and conferences. His papers have been cited over 6860 times. He has been included in the Top One Percent of the World's Scientists and Academics according to Thomson Reuters' list in 2017, 2020, and 2022. His primary research interests are in antenna design, radar, and adaptive filters.

https://doi.org/10.1017/S175907872400103X Published online by Cambridge University Press